Acta Pharmaceutica Sinica B 2025;15(6):2867−2883

Chinese Pharmaceutical Association
Institute of Materia Medica, Chinese Academy of Medical Sciences

Acta Pharmaceutica Sinica B

www.elsevier.com/locate/apsb
www.sciencedirect.com

ORIGINAL ARTICLE

Self-degradable "gemini-like" ionizable lipid-mediated delivery of siRNA for subcellular-specific gene therapy of hepatic diseases

Qiu Wang[a,b], Bin Wan[a], Yao Feng[c], Zimeng Yang[a], Dan Li[d], Fan Liu[a], Ya Gao[a], Chang Li[a], Yanhua Liu[e], Yongbing Sun[f], Zhonggui He[a], Cong Luo[a,*], Jin Sun[a,*], Qikun Jiang[a,*]

[a]*Department of Pharmaceutics, Wuya College of Innovation, Shenyang Pharmaceutical University, Shenyang 110016, China*
[b]*Department of Biomedical Engineering, College of Future Technology, Peking University, Beijing 100871, China*
[c]*Kangya of Ningxia Pharmaceutical Co., Ltd., Yinchuan 750000, China*
[d]*Department of Pharmacy, Southwest Hospital, Army Medical University (Third Military Medical University), Chongqing 400038, China*
[e]*Department of Pharmaceutics, School of Pharmacy, Ningxia Medical University, Yinchuan 750004, China*
[f]*Pharmaceutical Engineering Center for Solid Preparation in Chinese Herbal Medicine, Jiangxi University of Traditional Chinese Medicine, Nanchang 330006, China*

Received 15 January 2025; received in revised form 20 March 2025; accepted 1 April 2025

KEY WORDS

Self-degradable "gemini-like" ionizable lipids;
Lipid nanoparticles;
siRNA delivery;
Gene therapy;
Liver macrophages targeting;
Hepatic diseases;
Acute liver injury;
Non-alcoholic steatohepatitis

Abstract Tailored lipid nanoparticles (LNPs)-mediated small interfering RNA (siRNA) nanomedicines show promise in treating liver disease, such as acute liver injury (ALI) and non-alcoholic steatohepatitis (NASH). However, constructing LNPs that address biosafety concerns, ensure efficient delivery, and target specific hepatic subcellular fractions has been challenging. To evade above obstacles, we develop three novel self-degradable "gemini-like" ionizable lipids (SS-MA, SS-DC, SS-MH) by incorporating disulfide bonds and modifying the length of ester bond and tertiary amino head. Our findings reveal that the disulfide-bond-bridged LNPs exhibit reduction-responsive drug release, improving both biosafety and siRNA delivery efficiency. Furthermore, the distance of ester bond and tertiary amino head significantly influences the LNPs' pK_a, thereby affecting endosomal escape, hemolytic efficiency, absorption capacity of ApoE, uptake efficiency of hepatocytes and liver accumulation. We also develop the modified-mannose LNPs (M-LNP) to target liver macrophages specifically. The optimized M-MH_LNP@TNFα exhibits potential in preventing ALI by decreasing tumor necrosis factor α (TNFα) levels in the macrophages, while

*Corresponding authors.
E-mail addresses: luocong@syphu.edu.cn (Cong Luo), sunjin@syphu.edu.cn (Jin Sun), jiangqk_student@aliyun.com (Qikun Jiang).

Peer review under the responsibility of Chinese Pharmaceutical Association and Institute of Materia Medica, Chinese Academy of Medical Sciences.

https://doi.org/10.1016/j.apsb.2025.04.003

MH_LNP@DGAT2 could treat NASH by selectively degrading diacylglycerol *O*-acyltransferase 2 (DGAT2) in the hepatocytes. Our findings provide new insights into developing novel highly effective and low-toxic "gemini-like" ionizable lipids for constructing LNPs, potentially achieving more effective treatment for hepatic diseases.

1. Introduction

In recent years, various liver diseases, including acute liver injury (ALI), non-alcoholic steatohepatitis (NASH) and hepatoma, have lacked satisfactory therapeutic outcomes owing to complex pathogenesis and absence of druggable targets[1-4]. ALI, an inflammatory disease, is closely associated with overproduced tumor necrosis factor α (TNFα) of liver macrophages[2,5]. Currently, some therapeutic strategies such as TNFα-antibody and small molecule inhibitors have been employed to impede ALI[2,5]. However, these modalities have poorly targeting liver towards macrophages, resulting in some undesired side effects[2]. NASH, a serious liver disorder characterized by steatosis, hepatocyte damage, inflammation, and different degrees of fibrosis, currently lacks approved clinical therapeutic agents for NASH due to incomplete understanding of its molecular progression mechanisms[3,4,6-8]. Many studies have linked NASH to fat accumulation[3,4,6-8]. The diacylglycerol *O*-acyltransferase 2 (DGAT2), a key enzyme in triglyceride synthesis, has been explored as a NASH target[6]. DGAT2 inhibitor has been regarded as a potential candidate for NASH and is presently in phase II clinical study[9]. Nevertheless, small molecule inhibitors face issues such as safety concerns and potential drug resistance in long-term administration. Given these limitations in current approaches to both ALI and NASH, it is urgent need to exploit more powerful and precise tools for treating these liver diseases effectively.

The small interfering RNA (siRNA)-based therapeutics have emerged as a powerful and precise tool for diverse diseases, particularly hepatic diseases, cancer and genetic disorders[10-13]. Nevertheless, the clinical practice of naked siRNA is challenging due to its instability, vulnerability to extracellular RNases, negative charge and large size, which impede cellular uptake[10-13]. Currently, lipid nanoparticles (LNPs)-mediated gene delivery has been recognized as a promising therapeutic option for diverse hepatic diseases, offering high cellular uptake efficiency, low immunogenicity and mature industrial manufacture technology[12-17]. Although promising, LNPs poses several obstacles such as high inflammatory response, undesired adverse events, low gene transfection efficiency and poor targeting of specific cells[18]. These limitations primarily stem from poor biodegradation, low lysosome escape efficiency of ionizable lipids and slow cargos release from LNPs[19-21]. Previous studies in our group[22,23] have proved that pro-drug nanoparticles introduced disulfide bonds have reduction-sensitive release characteristic, which improves the safety and effective of nanoparticles. Recently, researchers have introduced some biodegradable disulfide bonds into the structure of ionizable lipids to enhance their biosafety[24-25]. Additionally, studies have demonstrated that varying the distance between ester bonds and tertiary amino ester bonds can affect the pK_a value of lipid nanoparticles, influencing their lysosomal escape efficiency[26]. Consequently, developing novel ionizable lipids to construct LNPs is crucial for the safe and efficient delivery of siRNA, potentially revolutionizing treatment approaches for various diseases.

In this study, we design three novel self-degradable structurally symmetrical ionizable lipids with the same molecular weight by incorporating disulfide bonds and modifying the length of ester bond and tertiary amino head, resembling a gemini, hence namely "gemini-like" lipids, abbreviated as SS-MA, SS-DC, SS-MH (Fig. 1). These lipids are used to construct LNPs *via* the ethanol injection method for treating various liver disorders (Fig. 1). The advantages of "gemini-like" ionizable lipids mediated LNPs are as follows: (i) the disulfide-bonds are introduced in ionizable lipids, which promote the LNPs degrade under the action of glutathione (GSH) in the cytoplasm, achieving rapid release siRNA to cytoplasm, improving the gene delivery efficiency and reducing the side effects of LNPs *in vivo*; (ii) the pK_a is regulated by adjusting the distance between the tertiary amino heads and the ester bonds in the ionizable lipids, further regulating the lysosome escape efficiency of LNPs. To enhance liver macrophage targeting of LNPs, we prepare modified-mannose LNPs, with the optimized M-MH_LNP@TNFα demonstrating robust liver macrophage-specific targeting and potent therapeutic effects in ALI mouse models[26,27]. Additionally, the LNPs constructed using lipid SS-MH loading DGAT2 siRNA exhibit better therapeutic effects in the treatment of NASH than that MC3_LNP. More importantly, self-degradable "gemini-like" ionizable lipids-based LNPs not only improve the delivery efficiency of siRNA *in vivo*, but also enhance the biological safety of LNPs after high-dose and long-term administration. Overall, our work establishes proof for a safety delivery strategy with low inflammatory profiles, high gene transfection efficiency, and hepatic subcellular-specific targeting to treat liver-associated diseases.

2. Materials and methods

2.1. Materials

2,2′-Dithiodiethanol, methanesulfonyl chloride, 2-(methylamino) ethanol (1.3 mL, 16.15 mmol), 4-(methylamino) butan-1-ol (1.85 mL, 16.15 mmol), 6-(methylamino) hexan-1-ol and lauroyl chloride were obtained from Leyan (Shanghai, China). The myristoyl chloride and decanoyl chloride were supplied by Beijing TongGuang Fine Chemicals Company (Beijing, China). Dioleoyl-4-methyl-dimethylaminobutyric acid ester (DLin-MC3-DMA), 1,2-distearoyl-sn-glycero-3-phosphocholine (DSPC), 1,2-dimyristoyl-rac-glycero-3-methoxypolyethylene glycol-2000 (DMG-PEG$_{2K}$)

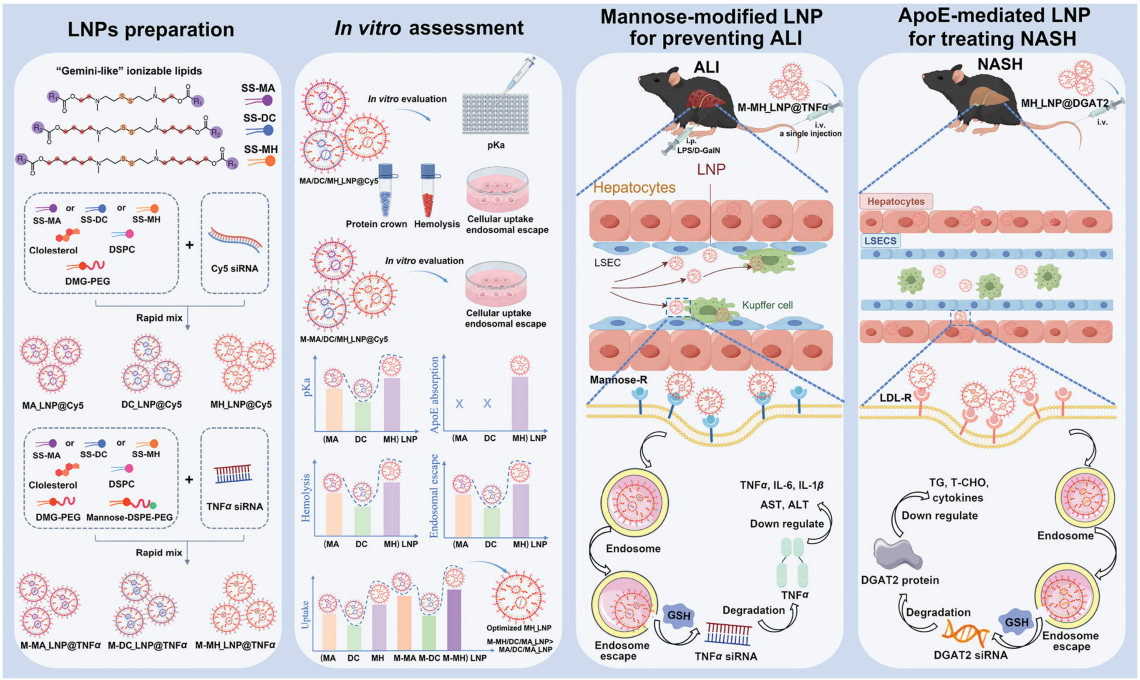

Figure 1 Schematic representation of the preparation process, *in vitro* assessment, anti-inflammatory effects and suppression of non-alcoholic steatohepatitis of "gemini-like" LNPs. Firstly, the unmodified/modified mannose "gemini-like" LNPs were constructed using ethanol injection method. Then, some *in vitro* assessments (pK_a, protein corona, hemolysis and cellular uptake, etc.) were conducted to optimize the "gemini-like" LNPs. Finally, we investigated the therapeutic effects of "gemini-like" LNPs against model mice established with acute liver injury and non-alcoholic steatohepatitis, respectively.

and cholesterol were purchased from AVT (Shanghai) Pharmaceutical Tech Co., Ltd. Mannose-modified 1,2-distearoyl-sn-glycero-3-phosphoethanolamine-N-[methoxy(polyethyleneglycol)-2000 (Man-DSPE-PEG_{2K}) was obtained from Xi'an ruixi Biological Technology Co., Ltd. (Xi'an, China). The siRNA sequences of tumor necrosis factorα (TNFα) and diacylglycerol *O*-acyltransferase 2 (DGAT2), and Cy5-labled siRNA were all available from GenePharma (Shanghai, China). Cell culture medium, fetal bovine serum (FBS), 3-(4,5-dimethylthiazol-2-yl)-2,5-diphenyltetrazolium bromide (MTT), Lyso-Tracker Green, and Hoechst were supplied by Dalian Meilun Biotech Co., Ltd. (Dalian, China). Vortex mixers and pipettes were provided by DLAB Scientific co., Ltd. (Beijing, China). Cell-culture dishes were brought from NEST Biotechnology (Wuxi, China). Lipofectamine™ 2000 and distilled water (RNase free) were brought from Thermo Fisher Scientific Inc. The Enzyme-Linked Immunosorbent Assay (ELISA) kits of mouse total cholesterol (T-CHO) and triglyceride (TG), D-(+)-galactosamine hydrochloride (D-GalN) and lipopolysaccharide (LPS) were supplied by Beijing Solarbio Science & Technology Co., Ltd. (Beijing, China). The ELISA kit of Interleukin-1β (IL-1β, abs520001) was obtained from Absin (Shanghai). Agarose, RNase A and Golden View were purchased from Beijing Biomed Gene Technology Co., Ltd. The test kits of aspartate aminotransferase (AST), alanine aminotransferase (ALT), UREA and Creatinine (CREA) were provided by Nanjing Jiancheng Bioengineering Institute. Apolipoprotein E (ApoE) and Proprotein Convertase Subtilisin/Kexin Type 9 (PCSK9) were purchased from Novoprotein (Shanghai, China). Primary antibody: TNF-α Rabbit pAb and DGAT2 Rabbit pAb, Secondary antibody: HRP Goat Anti-Rabbit IgG were purchased from ABclonal Biotechnology Co., Ltd. All other solvents or reagents used in this article were of analytical or HPLC grade.

2.2. *The synthesis of lipid SS-MA, SS-DC and SS-MA*

The synthetic rout of SS-MA, SS-DC and SS-MA was referenced a previous study[28]. 2,2′-Dithiodiethanol (3.02 g, 19.5 mmol) was dissolved in dry acetonitrile (30 mL), then added triethylamine (TEA, 8.1 mL, 58.5 mmol) and stirred for 5 min. Subsequently, the Methanesulfonyl chloride (MsCl, 4.5 mL, 58.5 mmol) was added dropwise to the reaction in an ice bath, and the reaction was gradually heated to 25 °C and stirred for 3 h. After the reaction, the crude product (SS-Ms) was extracted with ethyl acetate and water. Then, the pure SS-Ms was obtained by recrystallization method and the yield was 78.9%.

The SS-Ms (1.01 g, 3.23 mmol) was dissolved in acetonitrile (10 mL), and the K_2CO_3 was added for stirring (5 min). The same reaction was carried out three times. Next, the three reactions were added dropwise 2-(methylamino) ethanol (1.3 mL, 16.15 mmol), 4-(methylamino) butan-1-ol (1.85 mL, 16.15 mmol) or 6-(methylamino) hexan-1-ol (2.4 mL, 16.15 mmol) and stirred for 3 h at 25 °C, respectively. After the three reactions were completed, the products SS-OH (2), SS-OH (4) and SS-OH (6) were isolated and purified using silica gel column chromatography.

The SS-OH (2) (500 mg, 1.86 mmol), SS-OH (4) (500 mg, 1.54 mmol) or SS-OH (6) (500 mg, 1.31 mmol) was dissolved in dichloromethane (DCM, 10 mL) and the TEA (775, 341, and 183 μL) was added dropwise in an ice bath for stirring (5 min). Then, the myristoyl chloride (1.52 mL, 5.58 mmol), lauroyl chloride (1.1 mL, 4.62 mmol), and decanoyl chloride (815 μL, 3.93 mmol) were added to above three reactions for stirring (2 h), respectively. Subsequently, silica gel column chromatography was used to obtained pure SS-MA (60.1%), SS-DC (55.8%) and SS-

MH (49.7%). Furthermore, the HPLC was used to determine the purify of SS-MA, SS-DC and SS-MH. The conditions of chromatographic separation were as follows: Mobile phase A: acetonitrile (0.1% TFA); Mobile phase B: water (0.1% TFA); Gradient elution: 5% A to 100% A. The flow rate was set to 1.0 mL/min, and lipids were detected at wavelength 220 nm.

2.3. Screening of mass ratio of siRNA to lipids

The ethanol injection method was used to prepare the LNPs with different formulations and different mass ratio of siRNA to lipids. Among them, the Cy5-siRNA was selected as model siRNA, and the mass ratios of Cy5-siRNA to lipids were 1:20, 1:15 and 1:10, respectively. The SS-MA/DC/MH, DSPC, Cholesterol and DMG-PEG_{2K} (the molar ratio = 50:10:38.5:1.5) were dissolved in anhydrous ethanol. The Cy5-siRNA was dissolved in DEPC water containing citrate buffer solution (10 mmol/L, pH = 4.5). Then, the aqueous phase was added to ethanol phase with the volume ratio of 3 to 1 and vortexed for 30 min. Subsequently, the ethanol was removed using the ultrafiltration centrifugation method and obtained LNPs with different mass ratios of MA_LNP@Cy5, DC_LNP@Cy5 and MH_LNP@Cy5. The particle size and polydispersity index (PDI) of LNPs were characterized by Zetasizer (Malvern, UK). Furthermore, the encapsulation efficiency (EE) of Cy5-siRNA of MA_LNP@Cy5, DC_LNP@Cy5 and MH_LNP@Cy5 was determined by ultrafiltration centrifugation method. First, the LNPs were added to ultrafiltration centrifuge tube (100 kDa) and centrifuged 30 min (4000 rpm). Subsequently, we quantified the fluorescence intensity of Cy5-siRNA that had accumulated at the bottom of the centrifuge tube. Finally, the EE of Cy5-siRNA of LNPs was calculated according to Eq. (1):

$$EE = \frac{Fluorescence\ intensity\ of\ total\ Cy5\ siRNA - Fluorescence\ intensity\ of\ free\ Cy5\ siRNA}{Fluorescence\ intensity\ of\ total\ Cy5\ siRNA} \times 100\% \quad (1)$$

2.4. Construction of modified-mannose "gemini-like" LNPs

After optimizing the mass ratio of siRNA to total lipids (1:20), unmodified-mannose and modified-mannose "gemini-like" LNPs were prepared. For unmodified-mannose LNPs: the total lipids (SS-MA/DC/MH:DSPC:Cholesterol:DMG-PEG_{2K} = 50:10:38.5:1.5, molar ratio) were dissolved in anhydrous ethanol, the siRNA (Cy5-siRNA or TNFα-siRNA) was dissolved citrate buffer (RNase free, 10 mmol/L, pH 4.5); subsequently, the water phase and ethanol phase were rapidly mixed according to the volume ratio of 3:1 for vortexed (30 min); finally, the ethanol was removed by ultrafiltration centrifugation approach. For modified-mannose LNPs: The lipids compositions for 0.5%, 1% and 1.5% modified-mannose LNPs consisted of SS-MA/DC/MH, DSPC, Cholesterol, Man-DSPE-PEG_{2K} and DMG-PEG_{2K}, with molar ratios of 50:10:38.5:0.5:1.0, 50:10:38.5:1.0:0.5 and 50:10:38.5:1.5:0, respectively. The preparation protocol was identical to that for unmodified-mannose LNPs, except for incorporating Man-DSPE-PEG_{2K} to replace a portion or all of the DMG-PEG_{2K}. Consequently, 0.5%, 1%, and 1.5% mannose-modified LNPs were successfully prepared, designated as M-MA_LNP@Cy5, M-DC_LNP@Cy5, M-MH_LNP@Cy5, M-MA_LNP@TNFα, M-DC_LNP@TNFα, and M-MH_LNP@TNFα, respectively. The EE of LNPs encapsulating TNFα-siRNA was determined by applying Quant-iT RiboGreen Assay Kit. DLS was employed to detect the size, PDI and zeta potential of LNPs. The morphology of LNPs was observed using transmission electron microscopy.

2.5. In vitro siRNA release from LNPs

The *in vitro* release profile of siRNA from LNPs was evaluated by Centrifugal method. The MA_LNP@Cy5, DC_LNP@Cy5 and MH_LNP@Cy5 were incubated with PBS (pH 7.4) containing or without dithiothreitol (DTT, 10 mmol/L) in a constant temperature shaking table (37 °C), respectively. At pre-set timepoints, the samples were centrifuged (13,000 rpm, 10 min) and the supernatant was taken out. Then, the fluorescence intensity of supernatant was determined by microplate reader (Ex = 640 nm, Em = 680 nm).

2.6. The hemolysis of LNPs

The hemolysis assay was applied to investigate the capacity of LNPs to disrupt cell membranes under various pH conditions (5.0 and 7.4). First, the erythrocytes were collected from C57BL/6 mice plasma. Subsequently, the erythrocytes were diluted with PBS (pH 5.0, 7.4) to 2% suspension. The blank MA_LNP, DC_LNP and MH_LNP (200 μg/mL) were incubated with erythrocytes suspension (*v:v* = 1:1). Additionally, Triton X-100 (20%, *w/v*) solution and erythrocytes suspension were co-incubated as a positive control, the erythrocytes suspension was served as a negative control. After incubation, all samples were centrifuged (13,000 rpm, 5 min) and the absorbance of supernatant was measured by microplate reader (absorption wavelength = 540 nm). The hemolysis rate (HA) was calculated according to Eq. (2):

$$HA(\%) = \frac{A_t - A_n}{A_p - A_n} \times 100\% \quad (2)$$

HA represented hemolysis rate; A_t represented the absorbance of the samples to be tested; A_n represented the absorbance of negative control; A_p represented the absorbance of positive control.

2.7. Determination of apparent pK_a

The 6-(*p*-toluidino)-2-naphthalenesulfonic acid potassium salt (TNS) fluorescence probe was employed to determine the apparent pK_a of LNPs. First, the blank MA_LNP, DC_LNP and MH_LNP were diluted with a series of buffer solution with different pH (3−10) to 75 μmol/L. Next, the MA_LNP, DC_LNP and MH_LNP were incubated with TNS for 1 h in 37 °C shaking table and the final concentration of TNS was 0.6 μmol/L (n = 3). After incubation, the fluorescence intensity of each sample was measured by microplate reader (Ex = 321 nm, Em = 447 nm). The apparent pK_a value of LNPs was defined as the pH at which the fluorescence intensity of TNS reached half of its maximum value.

2.8. The protein corona of LNPs

The LNPs can be absorbed by the plasma proteins after intravenous administration, which significantly affect their surface properties and *in vivo* fate. Consequently, the specific plasma proteins adsorbed onto the LNP's surface were investigated by liquid chromatography/mass spectrometry (LC−MS/MS). First, the MA_LNP, DC_LNP and MH_LNP (1 mL) were incubated with mouse plasma (1 mL) in 37 °C shaker (1 h). After incubation, the samples were centrifuged (16,000×*g*, 30 min) and collected LNPs. Then, the LNPs were rinsed and dissolved using PBS (pH 7.4) for three times. Finally, the types and abundance of protein corona of LNPs were determined by LC−MS/MS, and the specific experimental operations were carried out by Novogene Co., Ltd.

2.9. Cytotoxicity

The RAW264.7 cells and HepG2 cells were inoculated into 96-well plates at a density of 5×10^3 and 3×10^3 cells/well, respectively. After incubation for 12 h, the spent culture medium was discarded, and the cells were subsequently incubated with fresh medium containing various concentration of MA_LNP, DC_LNP, MH_LNP and Lipo2000. After 48 h, the cell viabilities were evaluated using MTT assay.

2.10. Cellular uptake and internalized mechanism

The cellular uptake of LNPs was assessed by CSLM and flow cytometry. The HepG2 cells (2×10^5 cells/well) were inoculated into 24-well plates for overnight. Next, the cells were incubated with MA_LNP@Cy5, DC_LNP@Cy5 and MH_LNP@Cy5 (Cy5-siRNA, 100 nmol/L) for 4 h. Subsequently, the cells were rinsed with cold PBS, fixed with 4% paraformaldehyde and stained with Hoechst. Finally, the fluorescence intensity of Cy5-siRNA in cells was detected by CLSM.

For semi-quantitative analysis of cellular internalization, the HepG2 cells were cultured in 12-well plates at a density of 3×10^5 cells/well for 12 h. Thereafter, the cells were incubated with MA_LNP@Cy5, DC_LNP@Cy5 and MH_LNP@Cy5 (Cy5-siRNA, 100 nmol/L) for 4 h. After incubation, the cells were rinsed, digested, centrifuged and collected. Then, the fluorescent signal of Cy5-siRNA in cells was determined by flow cytometry.

Furthermore, flow cytometry was utilized to assess the cellular internalization mechanism of LNPs. The HepG2 cells (3×10^5 cells/well) were seeded into 12-well culture plates for 12 h. Afterwards, the cells were pre-treated with chlorpromazine (clathrin inhibitor, 5 μg/mL), indomethacin (caveolin inhibitor, 3 μg/mL) and colchicine (micropinocytosis inhibitor, 8 μg/mL) for 1 h, respectively. Then, the cells were incubated with MA_LNP@Cy5, DC_LNP@Cy5 and MH_LNP@Cy5 (Cy5-siRNA, 100 nmol/L) for 1 h. Finally, the cells were harvested and the fluorescent signal of Cy5-siRNA in cells was detected by flow cytometry.

Furthermore, we conducted an in-depth investigation to determine the role of ApoE in the targeting and uptake of LNPs. The HepG2 cells were cultured in 12-well plates at a density of 3×10^5 cells/well for overnight. Next, the cells were pre-incubated with DMEM medium or PCSK9 (1 μg/mL) for 2 h. Subsequently, the cells were continued to be incubated with MA_LNP@Cy5, DC_LNP@Cy5 and MH_LNP@Cy5 containing ApoE for 4 h. After incubation, the cells were rinsed, digested and collected for determining the fluorescent signal of Cy5-siRNA by flow cytometry.

2.11. Lysosome escape

The HepG2 cells (2×10^5 cells) were seeded into confocal dishes for 12 h. Then, naked Cy5-siRNA, MA_LNP@Cy5, DC_LNP@Cy5 and MH_LNP@Cy5 (Cy5-siRNA = 50 nmol/L) were used to incubate cells for 6 h respectively. After incubation, the cells were washed with PBS and stained with Lysotracker green and Hoechst. Subsequently, CLSM was applied to capture the fluorescence images of HepG2 cells.

2.12. Screening of DGAT2 siRNA sequences

To identify the potent gene sequence of DGAT2 siRNA, we strategically designed and designated three distinct siRNA sequences as Dgat2-Mus-405, Dgat2-Mus-602 and Dgat2-Mus-878. The AML-12 cells were seeded into 12-well plates at a density of 1×10^5 cells/well for 12 h. Thereafter, these cells were transfected with Lipo2000 wrapping DGAT2 siRNA for 24 h. Post-transfection, the cells were rinsed with cold PBS and harvested. The cells were then subjected to three cycles of freeze-thawing using liquid nitrogen, centrifuged, and the supernatant was carefully collected. Ultimately, the ELISA kit was used to determine the silencing efficiency of DGAT2 in AML-12 cells.

2.13. Preparation and characterization of LNPs encapsulated DGAT2 siRNA

Considering the outcomes related to endosome escape proficiency and cellular uptake efficiency, SS-MH was deemed the superior lipid candidate. Therefore, we constructed the LNPs (MH_LNP@DGAT2) encapsulating DGAT2 siRNA based on SS-MH. In addition, the LNPs (MC3_LNP@DGAT2) wrapping DGAT2 siRNA were prepared utilizing commercially available lipid DLin-DMA-MC3 as a comparative control. The preparation process of two LNPs was the same as the MA/DC/MH_LNP@Cy5 except for replacing Cy5-siRNA with DGAT2 siRNA. The particle diameter, PDI and zeta potential of MH_LNP@DGAT2 and MC3_LNP@DGAT2 were ascertained using Malvern. Furthermore, the morphological characteristics of the aforementioned LNPs were observed using Transmission Electron Microscopy (TEM).

2.14. In vitro gene silencing efficiency

The Western blot was used to investigate the *in vitro* gene silencing efficiency of MH_LNP@DGAT2 and MC3_LNP@DGAT2. The HepG2 cells were cultured in 12-well plates for 12 h. Afterwards, the cells were incubated with MH_LNP@DGAT2 and MC3_LNP@DGAT2 for 24 h, and the untreated group served as a control group. After incubation, cellular proteins were extracted, and the BCA assay kit was used to quantify the protein content. The proteins with the same concentration were then subjected to SDS-PAGE electrophoresis (100 V, 2 h). After electrophoresis, the proteins were transferred to PVDF membrane for 1 h (180 mA). The membrane was subsequently blocked with 5% skim milk for 1 h. Next, the membrane was incubated with DGAT2 anti-body at 4 °C for overnight. Finally, the membrane was incubated with secondary antibody for 1 h (25 °C) and the protein bonds were assayed using Gel Imager.

2.15. Animal studies

All experimental procedures were executed according to the protocols approved by Shenyang Pharmaceutical University Animal Care and Use Committee (SYPU-IACUC-C2021-6-1-096).

2.16. Biodistribution and liver microscopic imaging

The biodistribution of LNPs was evaluated using *In vivo* Imaging System (IVIS). The C57BL/6 mice were randomly divided into four groups ($n = 9$ for each group), and the Cy5-siRNA, MA_LNP@Cy5, DC_LNP@Cy5 and MH_LNP@Cy5 were injected intravenously at a dose of 0.75 mg/kg equivalent to Cy5-siRNA. At 4, 12 and 24 h post-administration, three mice from each treatment group were euthanized. Subsequently, the main organs (heart, liver, spleen, lung and kidney) of mice were excised and collected. Finally, the fluorescence intensity of these organs was quantified using IVIS system. Additionally, the liver (4 h post-administration) was rinsed with saline and then preserved in 4% paraformaldehyde in the dark. Subsequently, liver sections were prepared for fluorescent staining and scanned to investigate the distribution of LNPs within hepatocytes and live macrophages.

2.17. Anti-inflammatory efficacy

The C57BL/6 mice were employed to investigate anti-inflammatory efficacy of various formulations. In order to better investigate the therapeutic potential of the "gemini-like" LNPs, we prepared MC3_LNP based on the commercially available ionizable lipid MC3 (modified-mannose/unmodified LNP) as positive control. The mice were divided into 12 groups randomly ($n = 5$): normal mice (Control), LPS/D-GalN, naked TNFα, MA_LNP@TNFα, DC_LNP@TNFα, MH_LNP@TNFα, MC3_LNP@TNFα, M-MA_LNP@TNFα, M-DC_LNP@TNFα, M-MH_LNP@TNFα, M-MC3_LNP@TNFα and Magnesium isoglycyrrhizinate (MgIG). First, except for control and LPS/D-GalN groups, all the other groups of mice were injected intravenously with their respective formulations (250 μg/kg TNFα siRNA) and MgIG (4 mg/kg) respectively. At 24 h post-administration, all mice were intraperitoneally administrated with the mixture of LPS (5 μg/kg) and D-GalN (125 mg/kg) apart from control group. After 5 h, the blood samples were collected to measure the levels of TNF-α, IL-1β, and IL-6 in serum using ELISA kits. In addition, the levels of AST and ALT in serum were also determined to assess the hepatic function of mice.

2.18. Establishment of animal model of NASH

The animal model of NASH was established by feeding C57BL/6 mice high fat diet (60%) for 10 weeks. After 10 weeks, the blood and livers of three mice were harvested. Then, the serum was extracted to measure the levels of AST, ALT, IL-6, IL-1β, TNFα and T-CHO to validate whether the NASH model has been successfully established. Additionally, liver tissues were sliced and subjected to Oil Red O and Hematoxylin and eosin (H&E) staining for further histological analysis.

2.19. Anti-NASH efficacy

The anti-NASH efficacy of LNPs was investigated on high fat diet-induced C57BL/6 mice. The mice with NSAH were randomly divided into three groups ($n = 7$): saline group (Control), MH_LNP@DGAT2 and MC3_LNP@DGAT2 groups. First, the mice were intravenously administrated with saline, MH_LNP@DGAT2 and MC3_LNP@DGAT2 (DGAT2 siRNA = 1 mg/kg) for 8 weeks (administration twice a week), respectively. After 8 weeks, the serum, heart, liver, spleen, lung and kidney were collected. Next, the ELISA test kits were used to measure AST, ALT, TG, TNFα (JL10484, Jianglai biology, Shanghai), IL-6 (JL20268, Jianglai biology, Shanghai) and IL-1β levels. The hepatic gene silencing efficiency of DGAT2 was estimated using quantitative PCR (qPCR). The extent of hepatic steatosis and inflammation were evaluated by Oil Red O and H&E staining. Additionally, the levels of BUN and CREA in serum, and the H&E staining of heart, spleen, lung and kidney were used to access the *in vivo* safety of LNPs.

2.20. Bio-safety of high-dose blank LNPs

To explore whether ionizable lipids containing disulfide bonds can enhance the degradability of LNPs, the inflammatory response induced by high-dose LNPs was evaluated in C57BL/6 mice. First, the healthy C57BL/6 mice were divided into three groups ($n = 5$): saline (Control) group, MH_LNP and MC3_LNP groups. Then, the each of mice was intravenously injected saline (200 μL), MH_LNP and MC3_LNP (10 mg/kg, 200 μL), respectively. After 24 h, the blood of mice was collected and the ELISA kits were utilized to detect the levels of inflammatory factors including TNFα, IL-6 and IL-1β.

2.21. Statistical analysis

All data were calculated and assessed according to mean ± standard deviation (SD). Two tailed *t*-test or one-way analysis of variance (ANOVA) were applied to analyze the differences between comparative groups. The significant differences between the data were estimated at $P < 0.05$.

3. Results and discussion

3.1. Rational design and synthesis of "gemini-like" ionizable lipids

In this study, we rationally designed a series of novel ionizable lipids based on tertiary amino heads, the linker of disulfide bonds and alkane tails (Fig. 2A). We then synthesized three representative "gemini-like" ionizable lipids with symmetrical structures and identical molecular weight but varying distance between ester bonds and tertiary amino heads. These symmetric, disulfide-bridged lipids were designated as SS-MA, SS-DC, and SS-MH, each featuring different distances between tertiary amine heads and ester bonds. The detailed synthetic procedures for these three "gemini-like" ionizable lipids were outlined in Supporting Information Figs. S1−S3. The structures of SS-MA, SS-DC, and SS-MH were confirmed successfully using high-resolution mass spectrometry (HRMS) and proton nuclear magnetic resonance (^{1}H NMR) spectroscopy (Supporting Information Figs. S4−S9). In addition, the purity of three "gemini-like" lipids was more than, meeting the requirements of the follow-up experiments (Supporting Information Fig. S10).

3.2. Screen optimal mass ratio of total lipids and Cy5-siRNA

The LNPs with different mass of total lipids and siRNA were constructed using the ethanol injection method. The size, PDI and

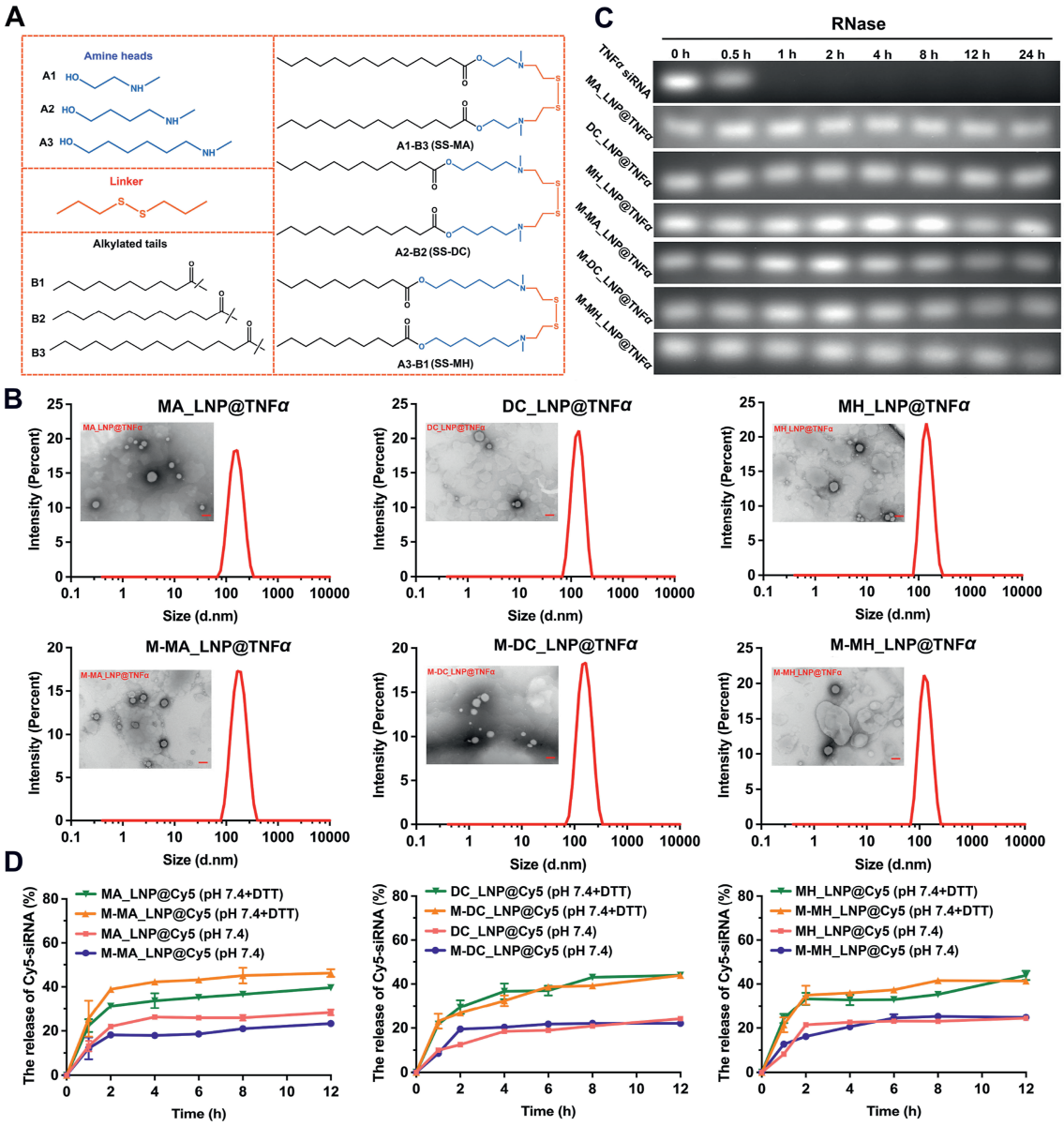

Figure 2 Characteristics of LNPs with different formulations. (A) The devised structures of biodegradable "gemini-like" ionizable lipids. (B) The size distribution profile and TEM images of LNPs with different formulations (scale bar = 100 nm). (C) Determination the stability of LNPs in the presence of RNase within 24 h using agarose gel electrophoresis. (D) The *in vitro* release behavior of Cy5-siRNA from different LNPs in pH 7.4 PBS with/without 10 mmol/L DTT within 12 h (n = 3 biologically independent samples).

EE of LNPs were exhibited in Supporting Information Table S1. It was found that LNPs had smaller size, lower PDI, as well as higher EE when the mass ratio of total lipids to Cy5-siRNA was optimized at 20:1. Consequently, the 20:1 mass ratio (total lipids:Cy5-siRNA) was deemed the optimal formulation for subsequent investigation.

3.3. Preparation and characterization of LNPs encapsulating TNFα siRNA

The optimal TNFα siRNA sequence was applied to construct the LNPs according to our previous study[29]. The size, PDI and EE of MA_LNP@TNFα, DC_LNP@TNFα and MH_LNP@TNFα are illustrated in Supporting Information Table S2. To improve liver macrophage targeting, we prepared LNPs modified with varying molar ratios of mannose. As shown in Supporting Information Table S3, the size of LNPs gradually enlarged with molar amounts of Man-DSPE-PEG_{2K}, but the difference between 0.5% and 1% modifications was less than 50 nm. Notably, the LNPs modified with 1% mannose exhibited superior liver macrophage targeting efficacy compared to those modified with 0.5% mannose (Supporting Information Fig. S11). Therefore, LNPs with 1% Man-DSPE-PEG_{2K} was selected as optimal formulation for further exploration. As exhibited in Fig. 2B, the sizes of MA/DC/MH_LNP@TNFα and 1% modified-mannose MA/DC/MH (M-MA/DC/MH) LNP@TNFα were all less than 200 nm, with the zeta potentials ranging from approximately +4−10 mV (Supporting Information Fig. S12), and the EE exceeding 95%

(Tables S2 and S3). The above LNPs were spherical with uniform size (Fig. 2B) and remained stable at 4 °C for 7 days (Supporting Information Fig. S13). Furthermore, it is important to ascertain whether siRNA in the MA/DC/MH_LNP@TNFα and M-MA/DC/MH_LNP@TNFα could keep intact in the presence of RNase. As shown in Fig. 2C, TNFα siRNA encapsulated in all six types of LNPs resisted RNase degradation for 24 h, while naked TNFα siRNA was degraded within 0.5 h. These results demonstrate that LNPs were able to protect siRNA from degradation.

3.4. *In vitro release of siRNA from LNPs*

In vitro release behavior of siRNA in different medium was accessed by microplate reader. As shown in Fig. 2D, the Cy5-siRNA release from both MA/DC/MH_LNP@Cy5 and M-MA/DC/MH_LNP@Cy5 was significantly enhanced in PBS (pH 7.4) supplemented with DTT (10 mmol/L) compared to PBS without DTT. These results suggest that all LNPs exhibited reduction-sensitive siRNA release characteristics, attributed to the disulfide bonds incorporated into the ionizable lipid structure. This feature was particularly beneficial for siRNA release in the cytoplasm with high GSH environment, potentially enhancing gene silencing efficiency. Notably, there was no significant difference observed in the cumulative siRNA release between modified-mannose and unmodified LNPs across various release media, indicating that the mannose modification on the surface of LNPs did not affect siRNA release kinetics.

3.5. *Apparent pK_a of blank LNPs*

The pK_a of LNPs is a critical factor influencing their lysosomal escape ability *in vivo*. Previous research has shown that the pK_a of vehicles in the range of 6.2−6.5 is particularly effective for siRNA/mRNA delivery[30]. As illustrate in Fig. 3A−C, an increase in the pK_a values of MA_LNP, DC_LNP, and MH_LNP with the elongation of the distance between the tertiary amine group and the ester bond in the ionizable lipid. Specifically, the pK_a values were approximately 5.2, 6.0, and 6.2 for MA_LNP, DC_LNP, and MH_LNP, respectively. Notably, the pK_a of MH_LNP fell within the ideal range for delivery vectors, suggesting that it might possess superior endosomal escape ability compared to the other formulations.

3.6. *Protein crown of LNPs*

LNPs can absorb the proteins in the plasma to form protein crown due to the high Gibbs free energy of LNPs, resulting in different biological behaviors *in vivo*. To better understand the biological behavior of blank MA/DC/MH_LNP, LC−MS/MS was applied to explore the specific proteins that adsorbed on the surface of LNPs. As shown in Fig. 3D−F, albumin was identified as the predominant protein adsorbed onto all three LNP formulations. Previous studies have shown that LNPs can target hepatocytes by binding to low-density lipoprotein receptors (LDL-R) after absorbing apolipoprotein E (ApoE) from plasma. Notably, among the top 20 absorbed proteins, blank MH_LNP exhibited a high affinity for ApoE (Fig. 3F), suggesting that it might predominantly target hepatocytes *via* an ApoE-mediated endocytosis mechanism. These findings demonstrate that the structural differences among SS-MA, SS-DC, and SS-MH lead to distinct protein corona compositions, which in turn may affect the *in vivo* fate of the respective LNPs. Research has revealed that liver-targeting LNPs have a pK_a value close to 6.4, which is related to the adsorption of ApoE on the surface of LNPs[31]. The difference in pK_a values can affect the distribution of LNPs in different organs, consequently impacting influencing the composition of their adsorbed protein corona[31]. The three types of "gemini-like" LNPs possess different pK_a. Based on this, we conclude that the pK_a value is important property influencing the adsorption of various proteins on the surface of "gemini-like" LNPs.

3.7. *Cell viability*

MTT assay was employed to evaluate the *in vitro* safety of LNPs against RAW264.7 and HepG2 cells. Lipofectamine 2000, a widely-used commercial gene transfection reagent, exerted a significant inhibitory effect on both RAW264.7 and HepG2 cells within the concentration range of 50−100 ng/mL (Supporting Information Fig. S14). In contrast, both unmodified and modified-mannose MA/DC/MH_LNPs maintained cell viability close to 100% across the tested concentration range. Lipofectamine 2000 exhibited noticeable cytotoxicity at concentrations exceeding 20 ng/mL. These results demonstrate that our self-degradable "gemini-like" LNPs possessed superior biosafety compared to Lipofectamine 2000, highlighting their potential as safer alternatives for gene delivery applications.

3.8. *Cellular internalization of LNPs*

The cellular uptake of "gemini-like" LNPs in RAW264.7 cells was estimated by CLSM. As exhibited in Fig. 4A, MH_LNP@Cy5 exhibited higher cellular uptake efficiency than MA/DC_LNP@Cy5 at both 2 and 4 h. Notably, modified-mannose LNPs showed stronger fluorescence signal than their unmodified counterparts, enhanced cellular internalization efficiency due to the binding interaction between mannose ligands and receptors (Fig. 4A and Supporting Information Fig. S15). The cellular uptake efficiency of LNPs in RAW264.7 cells followed the order of M-MH_LNP@Cy5 > M-MA_LNP@Cy5 > M-DC_LNP@Cy5 > MH_LNP@Cy5 > MA_LNP@Cy5 > DC_LNP@Cy5. Furthermore, flow cytometry was applied to analyze quantitatively the cellular uptake of LNPs in RAW264.7 cells (Supporting Information Fig. S16). The results were well consistent with the analytical results of CLSM.

We further investigated the internalization mechanism of our LNPs in hepatocytes using HepG2 cells, which highly express LDL receptors. As presented in Fig. 4B−D, the internalization process of MA_LNP, DC_LNP and MH_LNP predominantly facilitated by clathrin-mediated endocytosis and micropinocytosis. Furthermore, the cells transfected at 4 °C displayed very low fluorescence intensity, suggesting that internalization of LNPs was strictly dependent on energy. Given that ApoE can bind to LNPs in circulation and interact with receptors like LDL-R to facilitate liver targeting, we explored the role of ApoE in LNP delivery efficiency *in vitro*. As demonstrated in Fig. 4B−E, MA/DC/MH_LNPs exhibited enhanced cellular internalization in the presence of ApoE. However, this effect was negated when both PCSK9 (an LDL receptor binder) and ApoE were present, highlighting ApoE's crucial role in LNP-mediated siRNA delivery to hepatocytes. Notably, MH_LNP showed superior cellular uptake in HepG2 cells compared to DC_LNP and MA_LNP, possibly attributed to its increased surface adsorption of ApoE.

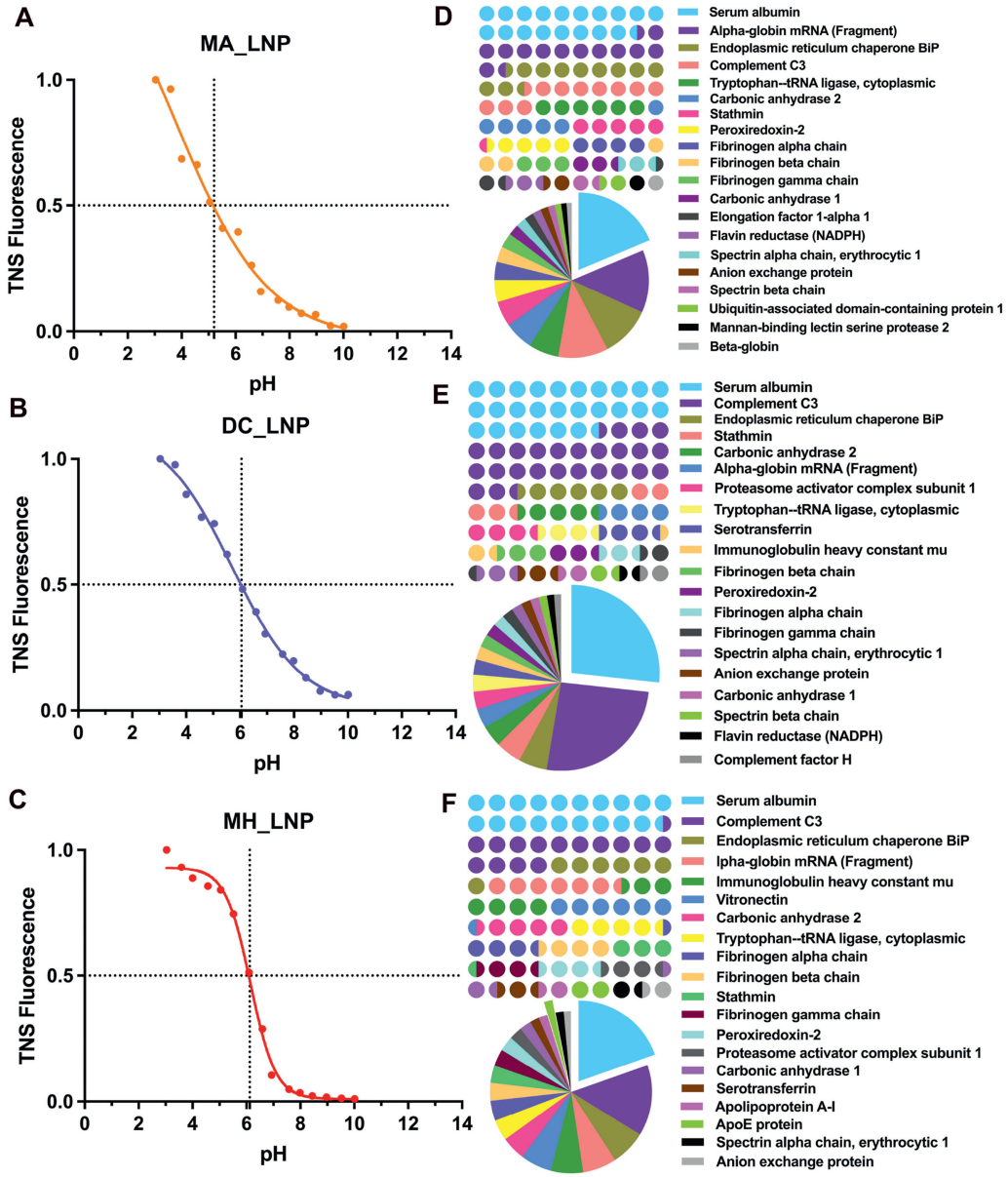

Figure 3 The pK_a value and protein corona assay of blank "gemini-like" LNPs. (A−C) The apparent pK_a determination of blank "gemini-like" LNPs using TNS assay. (D−F) The top 20 most abundant corona proteins were identified in the protein corona of different blank LNPs by LC−MS/MS method.

3.9. In vitro gene silencing

The TNFα siRNA silencing efficiency *in vitro* was evaluated by TNFα ELISA and Western blot methods. As depicted in Fig. 4E, both unmodified (MA/DC/MH_LNP@TNFα) and modified-mannose (M-MA/DC/MH_LNP@TNFα) formulations significantly inhibited TNFα secretion by RAW264.7 cells compared to naked TNFα siRNA groups. The modified-mannose LNPs demonstrated enhanced TNFα silencing efficiency, likely due to their improved targeting ability. Among the modified formulations, M-MH_LNP@TNFα exhibited the highest TNFα silencing efficiency, outperforming M-MA_LNP@TNFα and M-DC_LNP@TNFα, which can be attributed to its enhanced endosomal escape and cellular uptake efficiency. In addition, the Western blot analysis indicated that M-MH_LNP@TNFα more effectively downregulated the expression of TNFα, which was consistent with the results of ELISA (Fig. 4F).

3.10. Endosomal escape of LNPs

Rapid escape of siRNA from endosomes is of great significance for efficient gene silencing. The intracellular trafficking process of MA/DC/MH_LNP@Cy5 was explored using CLSM. As demonstrated in Supporting Information Fig. S17, naked Cy5-siRNA exhibited the highest level of co-localization with endosomes. Notably, MH_LNP@Cy5 demonstrated superior endosomal escape ability compared to MA_LNP@Cy5 and DC_LNP@Cy5, attributed to its optimal apparent pK_a of 6.2. To quantitatively assess endosomal escape, we calculated the Pearson's correlation coefficient between endosomes and Cy5-siRNA for the various

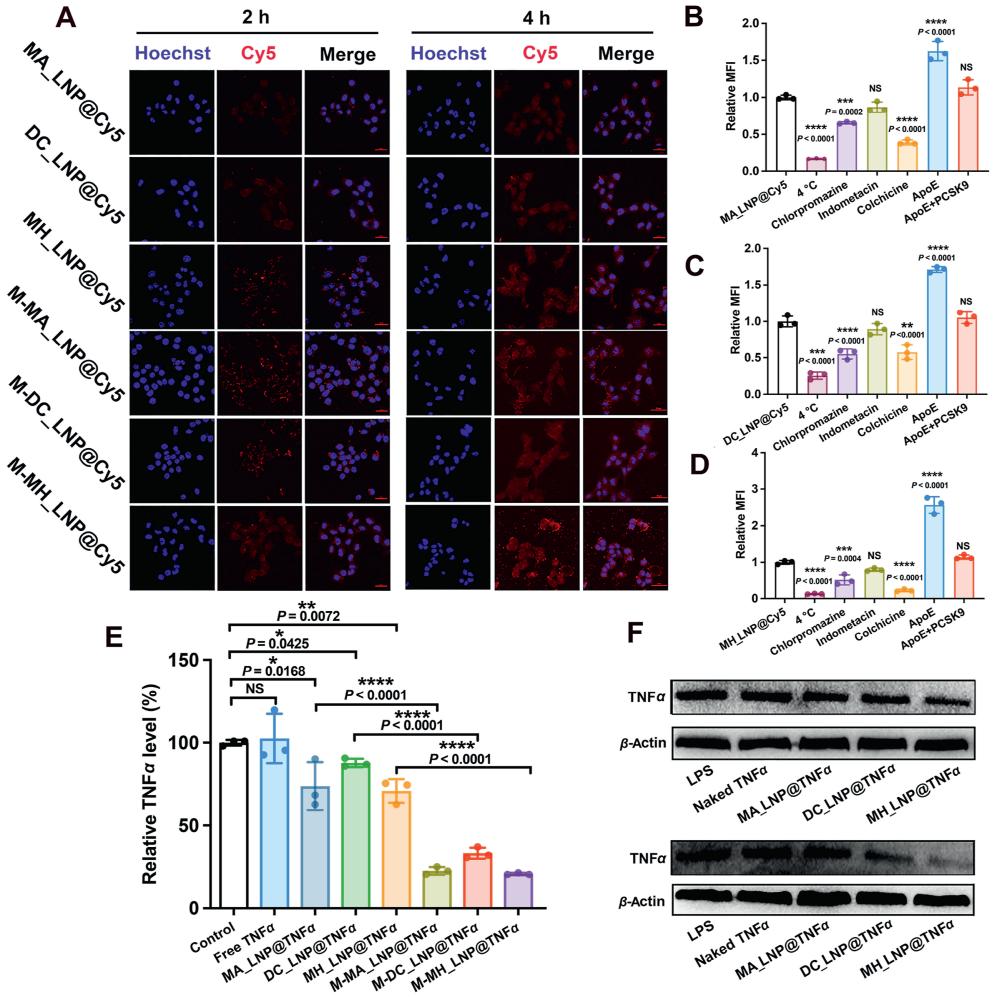

Figure 4 The cellular internalization, mechanism and *in vitro* gene silencing efficiency of LNPs. (A) Confocal imaging of MA/DC/MH@Cy5 and M-MA/DC/MH@Cy5 in RAW264.7 cells at both 2 and 4 h (scale bar = 25 μm). (B−D) The endocytosis performance of MA_LNP@Cy5, DC_LNP@Cy5 and MH_LNP@Cy5 in the presence of various inhibitors on HepG2 cells for 2 h (n = 3 biologically independent samples). (E) *In vitro* gene silencing efficiency of different LNPs against RAW264.7 cells treated with LPS (n = 3 biologically independent samples). (F) Western blot assays of TNFα in RAW264.7 cells. β-actin was used as a control. Data of (B−E) are presented as mean ± SD. The one-way ANOVA was used to determine the significance of the comparisons of data indicated in (B−E). *P < 0.05; **P < 0.01; ***P < 0.001, ****P < 0.0001. NS, not significance.

formulations (Supporting Information Fig. S18). The endosomal escape ability was the worst when the Pearson's correlation coefficient was 1. These results revealed that endosomal escape ability of aforementioned-LNPs were according to the following order: MH_LNP@Cy5 > MA_LNP@Cy5 > DC_LNP@Cy5 (Fig. S18).

3.11. *Hemolysis*

The hemolysis test was additionally employed to evaluate the disruptive effect of LNPs on cell membranes, thereby providing further insights into their endosomal escape capabilities. As exhibited in Supporting Information Fig. S19, the solution color progressively darkened with increasing concentrations of MA/DC/MH_LNPs in pH 5.0 PBS, indicating an increase in erythrocyte rupture. Notably, MH_LNP exhibited a more pronounced hemolytic effect than MA_LNP and DC_LNP at pH 5.0, aligning with the lysosomal escape results. In contrast, when incubated with LNPs in pH 7.4 PBS, the solution color remained largely unchanged, with most erythrocytes settling at the bottom of tube. These findings demonstrate that our LNPs could effectively disrupt endosomal membranes within a specific concentration range while sparing normal cell membranes, thus highlighting their favorable biosafety profile.

3.12. *In vivo biodistribution*

The *in vivo* biodistribution behavior of modified/un-modified mannose LNPs was assessed by IVIS imaging. As exhibited in Fig. 5A−C, the naked Cy5-siRNA solution showed greater accumulation in kidney than other LNPs administration groups, which could be attributed to the renal clearance of unencapsulated siRNA. At post 4 h intravenous injection, mannose-modified LNPs displayed stronger fluorescence signal in liver than their unmodified counterparts, suggesting that the mannose modification on the surface of LNPs could enhance accumulation of siRNA

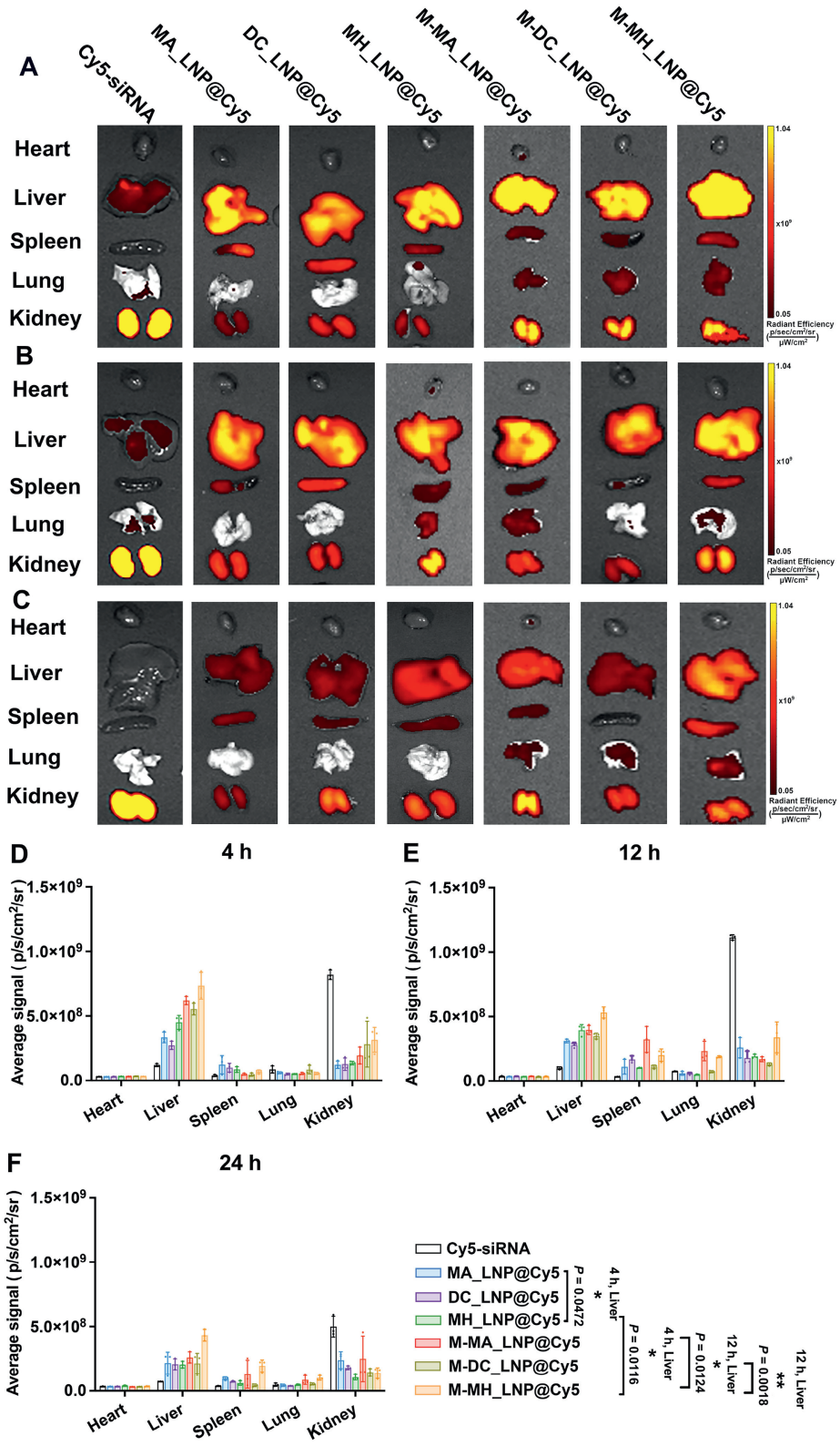

Figure 5 The *in vivo* biodistribution of different LNPs in C57BL/6 mice. *Ex vivo* fluorescence imaging of heart, liver, spleen, lung and kidney at 4 h (A), 12 h (B) and 24 h (C); (0.75 mg/kg Cy5-siRNA, $n = 3$ biologically independent animals). The semi-quantitative analysis fluorescence intensity of biodistribution of different LNPs at 4 h (D), 12 h (E) and 24 h (F); ($n = 3$ biologically independent animals). Data are shown as mean ± SD. The one-way ANOVA was used to determine the significance of the comparisons of data indicated in (D−F). *$P < 0.05$; **$P < 0.01$.

in the liver depending on the binding effect of mannose receptors. At post 12 h administration, M-MH_LNP@Cy5 showed increased accumulation in liver compared to M-MA_LNP@Cy5 and M-DC_LNP@Cy5, possibly due to facilitated hepatocellular internalization resulting in greater ApoE absorption *in vivo*. Additionally, the fluorescence semi-quantitative analysis results of tissue distribution at different time intervals were exhibited in Fig. 5D−F. These results elucidate that the LNPs formulated with SS-MH possessed significant advantages both *in vivo* and *in vitro*, positioning them as promising lipid candidates for future therapeutic applications.

3.13. Liver microscopic imaging of LNPs

The internalization of self-degradable "gemini-like" LNPs in hepatocytes and liver macrophages was further explored by liver microimaging technique. As illustrated in Supporting Information Fig. S20, MH_LNP@Cy5 exhibited higher internalization efficiency of hepatocytes than MA_LNP@Cy5 and DC_LNP@Cy5, probably due to its enhanced ApoE absorption capacity. In terms of liver macrophage uptake, modified-mannose LNPs exhibited improved *in vivo* internalization, which could be attributed to the active targeting afforded by mannose ligands (Supporting Information Fig. S21). Additionally, MH_LNP@Cy5 showed a notably higher uptake efficiency by liver macrophages than both MA_LNP@Cy5 and DC_LNP@Cy5. Among modified-mannose LNPs, M-MH_LNP@Cy5 exhibited superior uptake efficiency of liver macrophages compared to M-MA_LNP@Cy5 and M-DC_LNP@Cy5 (Fig. S21). The above results revealed that LNPs constructed with SS-MH had excellent properties in terms of hepatocytes and liver macrophages internalization *in vivo*, providing a foundation for the utilization of MH_LNP in therapeutic applications targeting liver diseases associated with hepatocytes and liver macrophages.

3.14. The prophylactic efficacy and safety evaluation of LNPs against ALI

The process of LNPs administration, model establishment of ALI, detection of inflammatory factors, and liver function indexes were conducted in a single injection according to our previous investigation protocol[29]. The schematic illustration of administration and establishment of ALI model was shown in Fig. 6A. In order to better validate the therapeutic effect of the "gemini-like" LNPs, we prepared MC3_LNP based on the commercially available ionizable lipid MC3 (modified-mannose/unmodified LNP) as positive control. As exhibited in Fig. 6B−F, compared with naked TNFα siRNA and LPS/D-GalN groups, all administration groups of LNPs and commercially available MgIG dramatically reduced the secretion of inflammatory cytokines (TNFα, IL-6 and IL-1β) and the levels of ASL and ALT. Notably, modified-mannose LNPs displayed superior suppression effects on ALI than unmodified LNPs and MgIG. In addition, the H&E staining results manifested that liver cells of mice treated with M-MH_LNP@TNFα and M-MC3_LNP@TNFα maintained normal morphology and abundant cytoplasm (Fig. 6G). Conversely, liver cells from mice treated with other formulations exhibited varying degrees of necrosis and nuclear disintegration (Fig. 6G). Remarkably, M-MH_LNP@TNFα exhibited excellent inhibition effect against ALI, which could be ascribed to the following reasons: (i) enhanced internalization efficiency in liver macrophages; (ii) superior endosomal escape ability; and (iii) rapid release of TNFα siRNA from M-MH_LNP@TNFα facilitated by the presence of cytoplasmic GSH.

Furthermore, H&E staining was applied to evaluate the biosafety of different formulations. As depicted in Supporting Information Fig. S22, compared with the control group (normal mice), no obvious histological morphology changes of main organs (heart, spleen, lung, kidney) was observed in the groups of LNPs and MgIG. Therefore, the H&E staining results demonstrate that the above LNPs possessed favorable biocompatibility *in vivo*.

3.15. Assessment of MH_LNP@DGAT2 in vivo and in vitro

NASH is a serious liver disorder characterized by fatty accumulation in hepatocytes and steatosis. Recently, there are no clinically approved drugs for the treatment of NASH. Therefore, developing drugs that target hepatocytes represents a highly promising therapeutic approach for NASH. The previous experimental results demonstrate that MH_LNP exhibited excellent liver accumulation and gene transfection efficiency *in vivo*. Hence, SS-MH was identified as optimal ionizable lipid to prepare LNPs encapsulating DGAT2 siRNA for treating NASH. Initially, three sequences of DGAT2 siRNA (Supporting Information Fig. S23) were designed and screened prior to LNP construction. Among these sequences, Dgat2-mus-405 showed significantly higher gene silencing efficiency *in vitro* than Dgat2-mus-602 and Dgat2-mus-878. As a result, Dgat2-mus-405 was regarded as perfect gene sequence for further exploration.

Subsequently, the MH_LNP@DGAT2 was constructed according to the same preparation process of MH_LNP@TNFα. Concurrently, the MC3_LNP@DGAT2 was formulated as a positive control. The size, morphology and zeta potentials of MH_LNP@DGAT2 and MC3_LNP@DGAT2 were illustrated in Supporting Information Figs. S24−S25. From the above results, MH_LNP@DGAT2 and MC3_LNP@DGAT2 both possessed uniform spherical structures with average particle diameter of approximately 168 and 205 nm, respectively. The zeta potentials of MH_LNP@DGAT2 and MC3_LNP@DGAT2 were determined to be around +7.44 and + 11.1 mV, respectively (Fig. S25). Moreover, we also investigated the DGAT2 siRNA degradation of LNPs under the action of RNase using agarose gel electrophoresis. The naked DGAT2 siRNA was completely degraded within 1 h, whereas the siRNA in MH_LNP@DGAT2 and MC3_LNP@DGAT2 remained largely intact for up to 24 h (Supporting Information Fig. S26). These findings suggest that MH_LNP@DGAT2 and MC3_LNP@DGAT2 exhibited strong resistance against siRNA degradation.

Next, the Western blot analysis was employed to appraise the gene silencing efficiency of MH_LNP@DGAT2 and MC3_LNP@DGAT2 in AML12 cells. As exhibited in Supporting Information Fig. S27, both MH_LNP@DGAT2 and MC3_LNP@DGAT2 significantly down-regulated DGAT2 expression compared to naked DGAT2 siRNA. These results indicated that the above two LNPs were capable of effectively silencing DGAT2 *in vitro*.

Afterwards, the animal model of NASH was established by inducing obesity, steatosis, and hepatic insufficiency in healthy C57BL/6 mice through a high-fat diet regimen. The schematic illustration of NASH model establishment and administration process is shown in Fig. 7A. As shown in Fig. 7B, the mice of high-fat diet (HFD) group exhibited higher body weight, liver weight, AST, ALT, T-CHO, TNFα, IL-6 and IL-1β compared to those in the normal-fat diet (NFD) group. These elevated parameters were attributed to hepatic fat accumulation induced by the

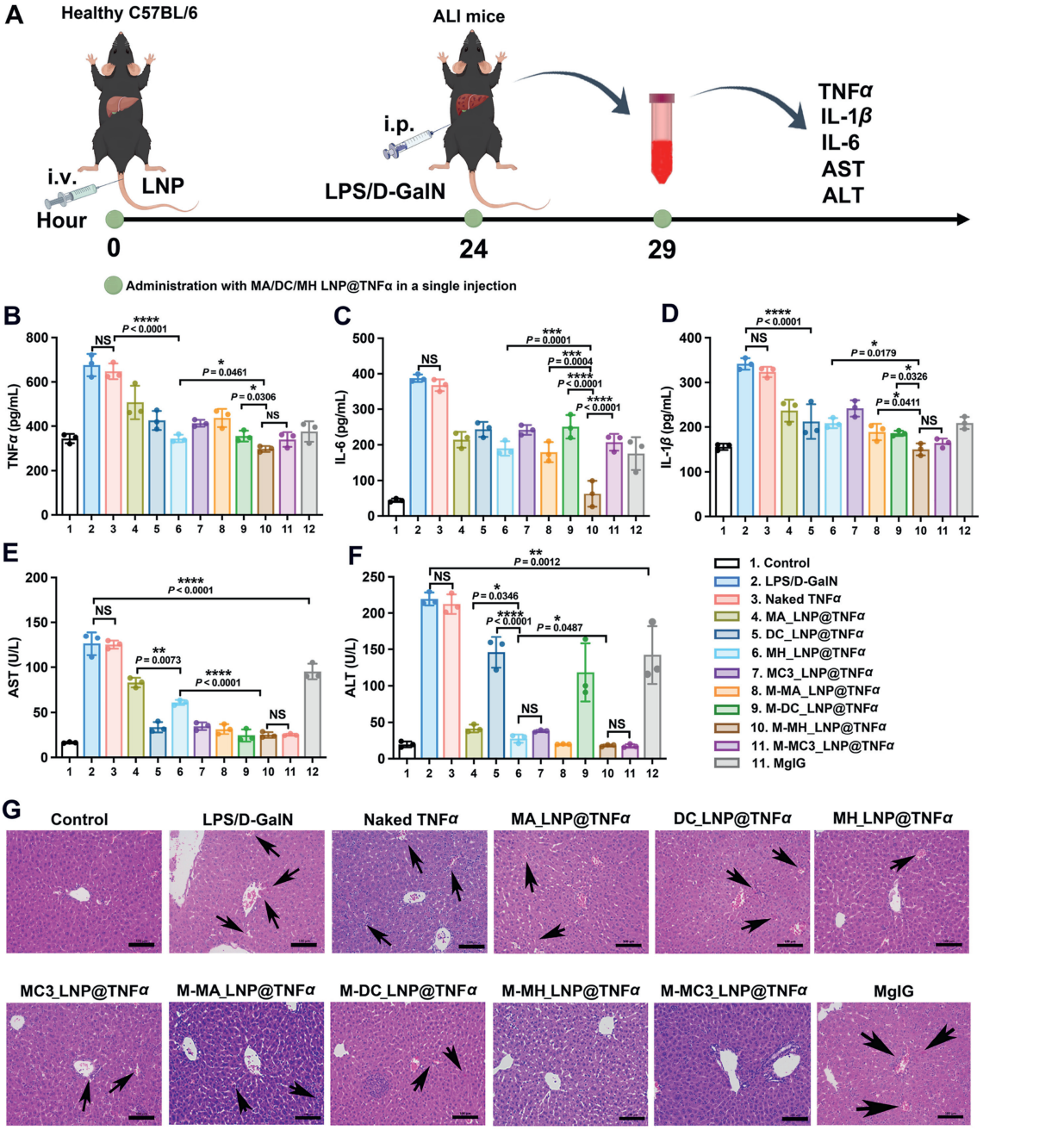

Figure 6 The prophylactic efficacy of "gemini-like" LNPs against ALI. (A) Schematic illustration of treatment in ALI. (B−F) The levels of inflammatory cytokine and liver function in mice serum were measured using ELISA ($n = 3$ biologically independent animals); TNFα (B), IL-6 (C), IL-1β (D), AST (E) and ALT (F). (G) H&E staining of liver slices was used to observe the liver injury of different administration groups (black arrow: inflammatory infiltration; scale bar = 100 μm). Data are exhibited as mean ± SD. The one-way ANOVA was used to determine the significance of the comparisons of data indicated in (B−F). *$P < 0.05$; **$P < 0.01$; ***$P < 0.001$, ****$P < 0.0001$. NS, not significance.

high-fat diet, resulting in hepatocyte damage and liver inflammation. Furthermore, histological analysis revealed pronounced hepatic lobular inflammation and steatosis in HFD mice, as evidenced by H&E and Oil Red O staining, respectively (Fig. 7C and D). Based on these findings and the pathological characteristics of NASH, the animal model of NASH was confirmed to be successfully established.

The therapeutic effect of LNPs encapsulating DGAT2 siRNA against NASH was evaluated following eight weeks of intravenous administration. As depicted in Fig. 7E−K, compared with saline, MH_LNP@DGAT2 and MC3_LNP@DGAT2 prominently reduced the level of AST, ALT, T-CHO, TG, TNFα, IL-6 and IL-1β in serum of NASH mice. The results indicated that LNPs encapsulating DGAT2 siRNA could decrease the levels of inflammatory cytokines (TNFα, IL-6 and IL-1β) and restore the normal liver function. Notably, MH_LNP@DGAT2 demonstrated superior efficacy in reducing AST, ALT, TG, and pro-inflammatory factor levels in mice. Conversely, the elevated aminotransferase and inflammatory cytokine levels observed in mice treated with MC3_LNP@DGAT2, which might be attributed

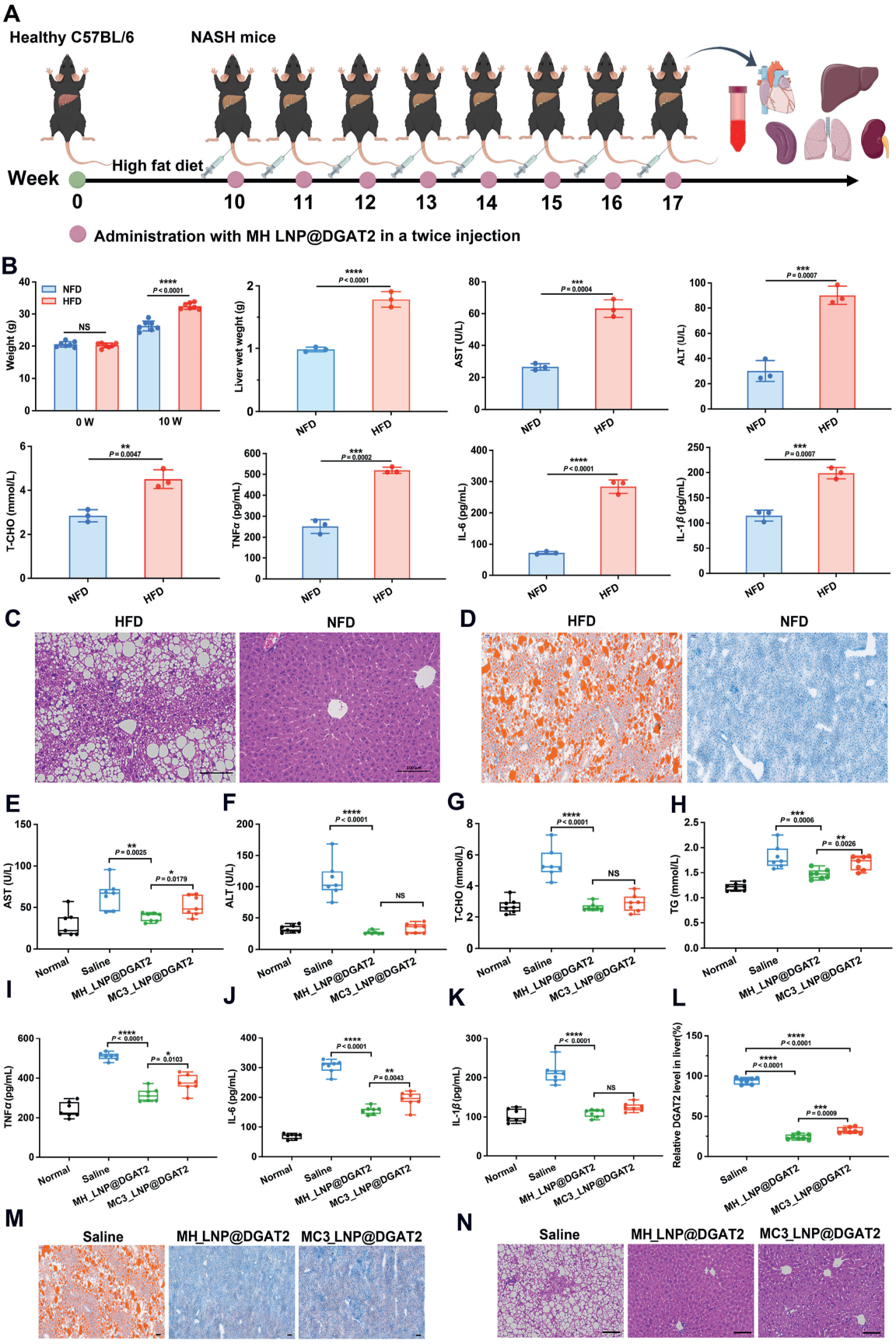

Figure 7 The animal model construction of NASH and the therapeutic effect of NASH *in vivo*. (A) The schematic illustration of NASH model construction and therapeutic process with MH/MC3_LNP@DGAT2. (B) Measure the body weight of mice fed HFD and NFD for 0 and 10 weeks

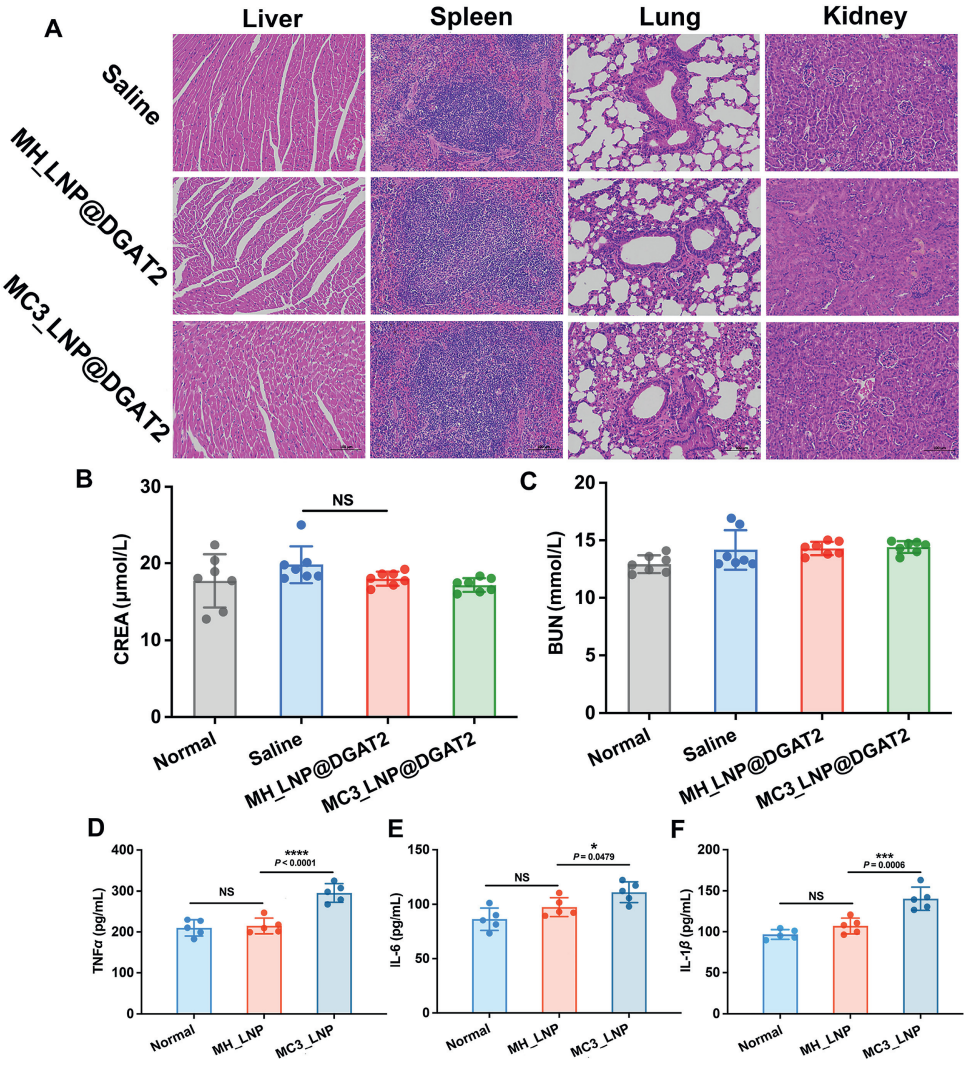

Figure 8 The biosafety evaluation of MH_LNP@DGAT2 and MC3_LNP@DGAT2 *in vivo* and inflammatory response of blank LNPs with high dose. (A) H&E staining of heart, spleen, lung and kidney of different administration groups (scale bar = 100 μm). (B, C) The levels of blood urea nitrogen (BUN) (B) and creatinine (CREA) (C) of different groups ($n = 7$, biologically independent animals). (D−F) Determine the levels of inflammatory cytokine in the serum of mice treated with high dose MH/MC3_LNP (10 mg/kg) using ELISA; TNFα (D), IL-6 (E) and IL-1β (F) ($n = 5$, biologically independent animals). Data are presented as mean ± SD. The one-way ANOVA was used to determine the significance of the comparisons of data indicated in (B, D, E and F). *$P < 0.05$; ***$P < 0.001$, ****$P < 0.0001$. NS, not significance.

to the inflammatory responses triggered by prolonged administration. In addition, the qPCR was utilized to determine the DGAT2 silencing efficiency of MH_LNP@DGAT2 and MC3_LNP@DGAT2 *in vivo*. As illustrated in Fig. 7L, the MH_LNP@DGAT2 and MC3_LNP@DGAT2 could dramatically reduce the level of DGAT2 mRNA compared to saline treatment. Intriguingly, MH_LNP@DGAT2 exhibited superior *in vivo* gene silencing efficiency, likely due to the rapid release of DGAT2 siRNA from MH_LNP@DGAT2 in response to the high levels of cytoplasmic GSH. Moreover, the hepatic steatosis and

($n = 10$, biologically independent animals); Liver wet weight in NFD and HFD groups ($n = 3$, biologically independent animals); The levels of AST, ALT, T-CHO, TNFα, IL-6 and IL-1β in serum of mice fed with NFD and HFD ($n = 3$, biologically independent animals). (C) HE staining of livers in HFD and NFD groups (scale bar = 100 μm). (D) Oil red O staining of livers in HFD and NFD group (scale bar: 100 μm). (E−K) Detect the levels of AST (E), ALT (F), T-CHO (G), TG (H), TNFα (I), IL-6 (J) and IL-1β (K) in serum of NASH mice administrated with MH_LNP@DGAT2 and MC3_LNP@DGAT2 (1 mg/kg DGAT2 siRNA; $n = 7$, biologically independent animals). (L) The DGAT2 gene silencing efficiency in the liver treated with MH_LNP@DGAT2 and MC3_LNP@DGAT2 ($n = 7$, biologically independent animals). The Oil Red O (M) and H&E (N) staining of different administration groups including saline, MH_LNP@DGAT2 and MC3_LNP@DGAT2 (scale bar = 100 μm). Data are expressed as mean ± SD. A two-tailed unpaired t-test was used to determine the significance of the comparisons of data indicated in (B). The one-way ANOVA was employed to determine the significance of the comparisons of data indicated in (E−L). *$P < 0.05$; **$P < 0.01$; ***$P < 0.001$, ****$P < 0.0001$. NS, not significance.

inflammation in mice were significantly ameliorated treated with MH_LNP@DGAT2 and MC3_LNP@DGAT2, as evidenced by Oil Red O and H&E staining results (Fig. 7M−N). Collectively, these results demonstrate that LNPs formulated with SS-MH effectively delivered DGAT2 siRNA to the liver and exhibited superior therapeutic efficacy compared to MC3_LNP.

The safety profile of MH_LNP@DGAT2 and MC3_LNP@DGAT2 in major organs was evaluated and presented in Fig. 8A−C. Histological analysis revealed no significant damage in the heart, spleen, lung, and kidney tissues of mice treated with LNP formulations compared to saline-treated controls. These findings demonstrate that both MH_LNP@DGAT2 and MC3_LNP@DGAT2 possessed favorable *in vivo* safety profiles, supporting their potential for further development as therapeutic agents.

3.16. Inflammatory response of blank LNPs with high dose

To further elucidate the *in vivo* safety profiles of MH_LNP and MC3_LNP, the inflammatory response elicited by high-dose administration of blank LNPs was evaluated by quantifying the serum levels of pro-inflammatory cytokines. As illustrated in Fig. 8D−F, high-dose MC3_LNP administration significantly elevated serum pro-inflammatory factor levels, indicating the induction of an inflammatory response in mice. In contrast, there were no significant differences in the levels of inflammatory cytokines between MH_LNP-treated group and control group. These findings suggested that MC3-based LNPs exhibited inferior biosafety at high doses (10 mg/kg), whereas the "gemini-like" ionizable lipids with disulfide bonds undergo GSH-mediated degradation, effectively mitigating LNP-induced inflammatory responses and enhancing overall biosafety. This improved safety profile of MH_LNP could be attributed to the incorporation of biodegradable disulfide bonds within the lipid structure.

4. Conclusions

In summary, three novel self-degradable "gemini-like" ionizable lipids (SS-MA, SS-DC, SS-MH) were rationally devised and synthesized for constructing LNPs to treat ALI and NASH. *In vitro* evaluations revealed that MH_LNP exhibited superior characteristics compared to MA_LNP and DC_LNP, including more appropriate pK_a, higher hemolytic efficiency, stronger ApoE absorption capacity, enhanced hepatocyte uptake efficiency, and improved liver accumulation. To optimize the therapeutic outcomes for ALI, modified-mannose LNPs encapsulating TNFα siRNA were developed to target specifically liver macrophages. Among these formulations, M-MH_LNP@TNFα demonstrated significantly superior suppression of ALI in mice compared to M-MA_LNP@TNFα and M-DC_LNP@TNFα. M-MH_LNP has higher siRNA delivery efficiency, which may be attributed to the increased apparent pK_a of LNPs as the distance between tertiary amino groups and ester bonds in the ionizable lipid structure is extended. In the chemical structures of three "gemini-like", oxygen, an electronegative atom, exerts an attractive force on the tertiary amine group, which in turn stabilizes the conjugate base of the ionizable lipid. The closer distance of the oxygen atom to the tertiary amine group, the greater the adsorption capacity, which in turn boosts the stability of the conjugate base, amplifies the acidity of the conjugate acid, and ultimately reduces the pK_a value. Consequently, an elongation of the distance between the ester bond and the tertiary amine results in a higher pK_a for the ionizable lipid. MH_LNP's pK_a value falls precisely within the optimal range (6.2−6.5), enabling more effective binding with ApoE and exhibiting superior hemolytic and lysosomal escape capabilities, thereby enhancing its *in vivo* gene silencing efficiency. Additionally, considering that hepatocyte-targeting ability of MH_LNP, we constructed MH_LNP encapsulating DGAT2 (MH_LNP@DGAT2) for treating NASH. As expected, the MH_LNP@DGAT2 displayed excellent therapeutic effect against NASH, comparable to that of MC3_LNP@DGAT2. Notably, MH_LNP showed superior *in vivo* biosafety than MC3_LNP (commercially available lipid) at high-dose administration (10 mg/kg), owing to its self-degradable ability under action of GSH. These findings collectively demonstrate that high-efficacy, low-toxicity "gemini-like" ionizable lipids represent promising candidates for delivering siRNA to specific liver cell populations, thereby facilitating effective treatment of liver diseases. The enhanced safety profile and targeted delivery capabilities of these novel LNPs offer significant potential for advancing therapeutic strategies in hepatic disorders.

Acknowledgements

This work was supported by National Key R&D Program of China (2021YFA0909900), Engineering Research Center of Tropical Medicine Innovation and Transformation of Ministry of Education (TMIT2024Y01, China), Liaoning Province Applied Basic Research Program (2022JH2/101300097, China), Liaoning Province Department of Education Project (LJKMZ20221365, China), National Postdoctoral Foundation of China (2023M730375), Postdoctoral Fellowship Program of China Postdoctoral Science Foundation (GZC20240050, China) and Outstanding youth fund of Shenyang Pharmaceutical University (YQ202208, China).

Author contributions

Qiu Wang, Qikun Jiang, Jin Sun and Cong Luo designed the research. Qiu Wang carried out the experiments and performed data analysis. Bin Wan, Yao Feng, Zimeng Yang, Dan Li, Fan Liu, Ya Gao and Chang Li participated part of the experiments. Jin Sun and Cong Luo provided experimental drugs and quality control. Qiu Wang wrote the manuscript. Qikun Jiang, Yanhua Liu, Yongbing Sun and Zhonggui revised the manuscript. All of the authors have read and approved the final manuscript.

Conflicts of interest

The authors have no conflicts of interest to declare.

Appendix A. Supporting information

Supporting information to this article can be found online at https://doi.org/10.1016/j.apsb.2025.04.003.

References

1. Allard J, Guillou D, Begriche K, Fromenty B. Drug-induced liver injury in obesity and nonalcoholic fatty liver disease. *Adv Pharmacol* 2019;**85**:75−107.
2. He H, Zheng N, Song ZY, Kim KH, Yao C, Zhang RJ, et al. Suppression of hepatic inflammation *via* systemic siRNA delivery by

memrane-disruptive and endosomolytic helical polypeptide hybrid nanoparticles. *ACS Nano* 2016;**10**:1859−70.
3. Musso G, Cassader M, Gambino G. Non-alcoholic steatohepatitis: emerging molecular targets and therapeutic strategies. *Nat Rev Drug Discov* 2016;**15**:249−74.
4. Zhou JE, Sun L, Liu L, Jia Y, Han Y, Shao J, et al. Hepatic macrophage targeted siRNA lipid nanoparticles treat non-alcoholic steatohepatitis. *J Control Release* 2022;**343**:175−86.
5. Ding F, Zhang HQ, Li Q, Yang CX. Identification of a potent ionizable lipid for efficient macrophage transfection and systemic anti-interleukin-1b siRNA delivery against acute liver failure. *J Mater Chem B* 2021;**9**:5136.
6. Yenilmez B, Wetoska N, Kelly M, Echeverria D, Min K, Lifshitz L, et al. Alterman, an RNAi therapeutic targeting hepatic DGAT2 in a genetically obese mouse model of nonalcoholic steatohepatitis. *Mol Ther* 2022;**30**:1329−42.
7. Ratziu V, Bellentani S, Cortez-Pinto H, Day C, Marchesini G. A position statement on NAFLD/NASH based on the EASL 2009 special conference. *J Hepatol* 2010;**53**:372−84.
8. Schuster S, Cabrera D, Arrese M, Feldstein AE. Triggering and resolution of inflammation in NASH. *Nat Rev Gastroenterol Hepatol* 2018;**15**:349−64.
9. Calle RA, Amin NB, Carvajal-Gonzalez S, Ross TT, Bergman A, Aggarwal S, et al. ACC inhibitor alone or co-administered with a DGAT2 inhibitor in patients with non-alcoholic fatty liver disease: two parallel, placebo-controlled, randomized phase 2a trials. *Nat Med* 2021;**27**:1836−48.
10. Hu B, Li B, Li K, Liu YY, Li CH, Zheng LL, et al. Thermostable ionizable lipid-like nanoparticle (iLAND) for RNAi treatment of hyperlipidemia. *Sci Adv* 2022;**8**:eabm1418.
11. Huang YY, Zheng SQ, Guo ZX, Mollerat du Jeu X, Liang XJ, Yang ZW, et al. Ionizable liposomal siRNA therapeutics enables potent and persistent treatment of Hepatitis B. *Signal Transduct Target Ther* 2022;**7**:38.
12. Liu SH, Liu J, Li HS, Mao KR, Wang HR, Meng XD, et al. An optimized ionizable cationic lipid for brain tumor-targeted siRNA delivery and glioblastoma immunotherapy. *Biomaterials* 2022;**287**:121645.
13. Zheng Q, Qin FM, Luo RJ, Jin CH, Huang H, Xi H, et al. mRNA-loaded lipid-like nanoparticles for liver base editing *via* the optimization of central composite design. *Adv Funct Mater* 2021;**31**:2011068.
14. Cheng Q, Wei T, Farbiak L, Johnson LT, Dilliard SA, Siegwart DJ. Selective organ targeting (SORT) nanoparticles for tissue-specific mRNA delivery and CRISPR−Cas gene editing. *Nat Nanotechnol* 2020;**15**:313−20.
15. Zong Y, Lin Y, Wei T, Cheng Q. Lipid Nanoparticle (LNP) enables mRNA delivery for cancer therapy. *Adv Mater* 2023;**35**:e2303261.
16. Su KX, Shi L, Sheng T, Yan XX, Lin LX, Meng CY, et al. Reformulating lipid nanoparticles for organ-targeted mRNA accumulation and translation. *Nat Commun* 2024;**15**:5659.
17. Wu SQ, Su KX, Yan XX, Shi L, Lin LX, Ren E, et al. Paracyclophane-based ionizable lipids for efficient mRNA delivery *in vivo*. *J Control Release* 2024;**376**:395−401.
18. Ndeupen S, Qin Z, Jacobsen S, Bouteau A, Estanbouli H, Bz Igyártó. The mRNA-LNP platform's lipid nanoparticle component used in preclinical vaccine studies is highly inflammatory. *iScience* 2021;**24**:103479.
19. Tanaka H, Sakurai Y, Anindita J, Akita H. Development of lipid-like materials for RNA delivery based on intracellular environment-responsive membrane destabilization and spontaneous collapse. *Adv Drug Deliv Rev* 2020;**154**:210−26.
20. Liu S, Cheng Q, Wei T, Yu X, Johnson LT, Farbiak L, et al. Membrane-destabilizing ionizable phospholipids for organ-selective mRNA delivery and CRISPR−Cas gene editing. *Nat Mater* 2021;**20**:701−10.
21. Wang M, Zuris JA, Meng F, Rees H, Sun S, Deng P, et al. Efficient delivery of genome-editing proteins using bioreducible lipid nanoparticles. *Proc Natl Acad Sci USA* 2016;**113**:2868−73.
22. Sun BJ, Luo C, Zhang XB, Guo MR, Sun MC, Yu H, et al. Probing the impact of sulfur/selenium/carbon linkages on prodrug nanoassemblies for cancer therapy. *Nat Commun* 2019;**19**:3211.
23. Sun BJ, Luo C, Yu H, Zhang XB, Chen Q, Yang WQ, et al. Disulfide bond-driven oxidation- and reduction-responsive prodrug nanoassemblies for cancer therapy. *Nano Lett* 2018;**18**:3643−50.
24. Akita H, Ishiba R, Hatakeyama H, Tanaka H, Sato Y, Tange K, et al. A neutral envelope-type nanoparticle containing pH-responsive and SS-cleavable lipid-like material as a carrier for plasmid DNA. *Adv Healthcare Mater* 2013;**2**:1120−5.
25. Tanaka H, Takahashi T, Konishi M, Takata N, Gomi M, Shirane D, et al. Self-degradable lipid-like materials based on "hydrolysis accelerated by the intra-particle enrichment of reactant (HyPER)" for messenger RNA delivery. *Adv Funct Mater* 2020;**30**:1910575.
26. Akita H, Noguchi Y, Hatakeyama H, Sato Y, Tange K, Nakai Y, et al. Molecular tuning of a vitamin E-scaffold pH-sensitive and reductive cleavable lipid-like material for accelerated *in vivo* hepatic siRNA delivery. *ACS Biomater Sci Eng* 2015;**1**:834−44.
27. Chu S, Tang C, Yin C. Effects of mannose density on *in vitro* and *in vivo* cellular uptake and RNAi efficiency of polymeric nanoparticles. *Biomaterials* 2015;**52**:229−39.
28. Jain P, Hung HS, Li BW, Ma JR, Dong DY, Lin XJ, et al. Zwitterionic hydrogels based on a degradable disulfide carboxybetaine cross-linker. *Langmuir* 2019;**35**:1864−71.
29. Wang Q, Jiang KQ, Li D, Yang ZM, Gao L, Liu F, et al. Elaborately engineering of lipid nanoparticle for targeting delivery of siRNA and suppressing acute liver injury. *Chin Chem Lett* 2024;**35**:108683.
30. Dong YZ, Siegwart DJ, Anderson DG. Strategies, design, and chemistry in siRNA delivery systems. *Adv Drug Deliv Rev* 2019;**144**:133−47.
31. Dilliard SA, Cheng Q, Siegwart DJ. On the mechanism of tissue-specific mRNA delivery by selective organ targeting nanoparticles. *Proc Natl Acad Sci U S A* 2021;**118**:e2109256118.